Oncogene (2017) **36**, 208–218

www.nature.com/onc

OPEN

ORIGINAL ARTICLE

Amplification of R-spondin1 signaling induces granulosa cell fate defects and cancers in mouse adult ovary

M-C De Cian[1,2,9], E Pauper[1,9], R Bandiera[3,9], VPI Vidal[1], S Sacco[1], EP Gregoire[1], A-A Chassot[1], C Panzolini[1], D Wilhelm[4], E Pailhoux[5], SA Youssef[6], A de Bruin[6,7], K Teerds[8], A Schedl[1], I Gillot[1] and M-C Chaboissier[1]

R-spondin1 is a secreted regulator of WNT signaling, involved in both embryonic development and homeostasis of adult organs. It can have a dual role, acting either as a mitogen or as a tumor suppressor. During ovarian development, *Rspo1* is a key factor required for sex determination and differentiation of the follicular cell progenitors, but is downregulated after birth. In human, increased RSPO1 expression is associated with ovarian carcinomas, but it is not clear whether it is a cause or a consequence of the tumorigenic process. To address the role of *Rspo1* expression in adult ovaries, we generated an *Rspo1* gain-of-function mouse model. Females were hypofertile and exhibited various ovarian defects, ranging from cysts to ovarian tumors. Detailed phenotypical characterization showed anomalies in the ovulation process. Although follicles responded to initial follicle-stimulating hormone stimulation and developed normally until the pre-ovulatory stage, they did not progress any further. Although non-ovulated oocytes degenerated, the surrounding follicular cells did not begin atresia. RSPO1-induced expression not only promotes canonical WNT signaling but also alters granulosa cell fate decisions by maintaining epithelial-like traits in these cells. This prevents follicle cells from undergoing apoptosis, leading to the accumulation of granulosa cell tumors that reactivates the epithelial program from their progenitors. Taken together, our data demonstrate that activation of RSPO1 is sufficient in promoting ovarian tumors and thus supports a direct involvement of this gene in the commencement of ovarian cancers.

Oncogene (2017) **36,** 208–218; doi:10.1038/onc.2016.191; published online 6 June 2016

INTRODUCTION

WNT/β-catenin (CTNNB1) signaling is involved in numerous biological processes from embryogenesis to stem cell activation. Deregulation of this pathway is responsible for many diseases, most notably colorectal cancer. Indeed, 90% of colorectal cancers result from APC mutations leading to the activation of this pathway.[1] WNT signaling is tightly controlled by negative and positive modulators like APC and R-spondins (RSPO), a family of four members of secreted proteins. Fusions of RSPO2 and RSPO3 activate WNT signaling in colorectal cancers,[2] and amplifications of *RSPO1* have been associated with 8% of ovarian epithelial cancers.[3,4] However, functional evidence for a direct involvement of *RSPO1* in ovarian tumor development is still missing.

Depending on the cell type, *Rspo1* may act either as a mitogen or a tumor suppressor:[5,6] variants of the *RSPO1* locus have been reported in ovarian cancers highlighting its role as an oncogene.[3,4] By contrast, *RSPO1* loss-of-function mutations predispose to squamous cell carcinoma.[6] On the molecular level, RSPO1 binds to the recruitment receptors LGR4, LGR5 or LGR6 leading to stabilization of CTNNB1, and in turn CTNNB1 interacts with transcription factors such as LEF/TCF in the nucleus and trans-activates target genes such as *Axin2* (for a model, see ref. 7).

CTNNB1 is not only a key factor of the WNT signal-transduction pathway, but is also a component of adherens junctions linking cadherins via α-catenin to the actin cytoskeleton at the plasma membrane of epithelial cells.[8] The membrane function of CTNNB1 can be partially substituted by the related protein JUP (Plakoglobin/γ-catenin), an important component of desmosomes that anchors epithelial cells to intermediate filaments and can also act as a signaling molecule at least *in vitro*.[9,10] Several studies support a role for JUP in cancer.[11] Although a direct link between RSPO1 and JUP has not yet been established, skin cells from patients affected by *RSPO1* loss-of-function mutations exhibit defects reminiscent of desmosome abnormalities.[6]

In addition to the skin diseases, such as palmoplantar hyperkeratosis, patients carrying mutations in *RSPO1* exhibit female-to-male sex reversal, and predisposition to squamous cell carcinoma and seminoma.[6,12] Using functional analysis in mice, the role of RSPO1 and canonical WNT signaling has been unraveled in female ovarian development.[13–15] Prior to sex determination, *Rspo1* is involved in the proliferation of progenitor cells that are located within the surface epithelium of the undifferentiated gonads.[16,17] Following sex determination, cells of the ovarian surface epithelium (OSE) continue to proliferate and enter the gonads to give rise to precursors of the granulosa cells.[18,19] At this stage, *Rspo1* is required to maintain granulosa precursors in the undifferentiated state.[14,20] Accordingly, LGR4- and LGR5-expressing precursor cells contribute to the formation of the follicle pool from which follicles are recruited

[1]University Nice Sophia Antipolis, Inserm, CNRS, iBV, Nice, France; [2]EA 7310, Université de Corte, Corte, France; [3]Wellcome Trust—Medical Research Council Cambridge Stem Cell Institute, University of Cambridge, Cambridge, UK; [4]Department of Anatomy and Neuroscience, University of Melbourne, Parkville Victoria, Australia; [5]UMR BDR, INRA, ENVA, Université Paris Saclay, Jouy-en-Josas, France; [6]Department of Pathobiology, Faculty of Veterinary Medicine, Dutch Molecular Pathology Center, Utrecht University, Utrecht, The Netherlands; [7]Department of Pediatrics, Division of Molecular Genetics, University Medical Center Groningen, Groningen, The Netherlands and [8]Department of Human and Animal Physiology, Wageningen University, Wageningen, The Netherlands. Correspondence: Dr I Gillot or Dr M-C Chaboissier, iBV, Institut Biologie Valrose, University Nice Sophia Antipolis, UFR Sciences, Parc Valrose, 28 Avenue Valrose, 06108 Nice cedex 2, France.
E-mail: gillot@unice.fr (IG) or marie-christine.chaboissier@unice.fr (M-CC)
[9]These authors contributed equally to this work.
Received 14 September 2015; revised 26 February 2016; accepted 21 April 2016; published online 6 June 2016

during reproductive life.[21] In mice, *Rspo1* expression becomes significantly downregulated in the first week *post partum*,[22] suggesting that RSPO1 is not required for the recruitment and maturation of follicles, and consequently proper ovarian functioning.

From the onset of puberty, the ovary undergoes successive cycles of follicular recruitment, maturation, OSE exfoliation, subsequent ovulation and *corpus luteum* (CL) formation.[23] Progesterone synthetized by the CL is necessary to prepare the uterine wall for implantation. LGR5-positive OSE cells are presumed to contribute to both post-ovulatory repair of the OSE[24] and, together with LGR4-positive lutein cells, progesterone production.[25,26] Activation of canonical WNT signaling must therefore be tightly controlled in the adult ovary. Consequently premature activation of canonical WNT signaling in differentiating granulosa cells leads to the appearance of precancerous follicle-like lesions around 6 weeks *post partum*, and 57% of these become granulosa cell tumors (GCTs) before the age of 7.5 months.[27]

In women, ovarian cancers derive from three major histotypes: surface epithelia, sex-chord stromal cells and germ cells.[28] Approximately 3% of ovarian cancers are derived from germ cells, 7% come from sex-chord stromal cells and 90% arise from OSE or fallopian tube epithelium.[28] GCTs are categorized into two distinct subtypes, the juvenile and the adult form.[29] Although less common than OSE-derived cancers in women, GCT frequently occurs in primates and domestic animals.[28] Moreover, in mouse models adult granulosa cells originate from two distinct waves of migration of progenitor cells of the OSE.[18] Given that (i) ectopic activation of canonical WNT signaling within the ovary has oncogenic effects,[27] (ii) RSPO1 is an activator of canonical WNT signaling during ovarian development[14] and (iii) *RSPO1* is amplified in ovarian cancers,[3] we hypothesized that RSPO1 misexpression could be a cause of ovarian defects and eventually cancer development. Using a gain-of-function mouse model (*Sf1:Cre*$^{Tg/+}$; *R26*$^{Rspo1/+}$), we show that *post partum* maintenance of *Rspo1* expression in somatic cells of the mouse ovary impairs homeostasis of the healthy ovary.

RESULTS

Rspo1 expression is downregulated in adult follicles

RSPO1/Rspo1 is highly expressed in somatic cells of the ovary during embryogenesis.[6,30] In the 2 weeks following birth, however, *Rspo1* expression is downregulated as evidenced by qRT–PCR analysis.[22] To obtain a more detailed expression profile and identify the cell types that express *Rspo1* late in development and during the postnatal period, we performed *in situ* hybridization experiments. Strong expression of *Rspo1* was found within the fetal ovary at 16.5 days post coitum (d*pc*), which significantly decreased after birth and remained at low levels in granulosa cells of cortical follicles in adult ovaries (Figures 1a–c). In contrast, *Rspo1* was robustly expressed in the OSE at all stages (Figures 1a–c). To understand whether RSPO1 was able to activate canonical WNT signaling, we next analyzed whether the *Axin2*$^{+/LacZ}$ reporter of this pathway[31] was expressed in the adult ovary. β-Galactosidase staining was detected in the OSE and in the ovarian stroma as well as in oocytes (Figures 1e–g). By contrast, granulosa cells were weakly stained after birth, indicating that RSPO1/WNT signaling is downregulated in this compartment of the follicle.

Increased RSPO1 expression activates canonical WNT signaling in adult ovaries

To assess the importance of *Rspo1* repression in the postnatal ovary, we next investigated the effect of induced *Rspo1* expression on ovarian homeostasis. To this end, we generated *Sf1-Cre*$^{Tg/+}$; *R26*$^{Rspo1/+}$ mice (Supplementary Figure S1). We first established the ability of female *Sf1-Cre*$^{Tg/+}$; *R26*$^{Rspo1/+}$ mice to ectopically express *Rspo1* throughout the ovary (Figures 1c and d). Next, we assessed that induced expression of *Rspo1* led to a strong, although variable, follicular activation of canonical WNT signaling by detecting β-galactosidase in ovaries from *Sf1-Cre*$^{Tg/+}$; *R26*$^{Rspo1/+}$; *Axin2*$^{+/LacZ}$ mice (Figures 1g and h). This confirmed that sustained expression of *Rspo1* activates canonical WNT signaling in ovaries.

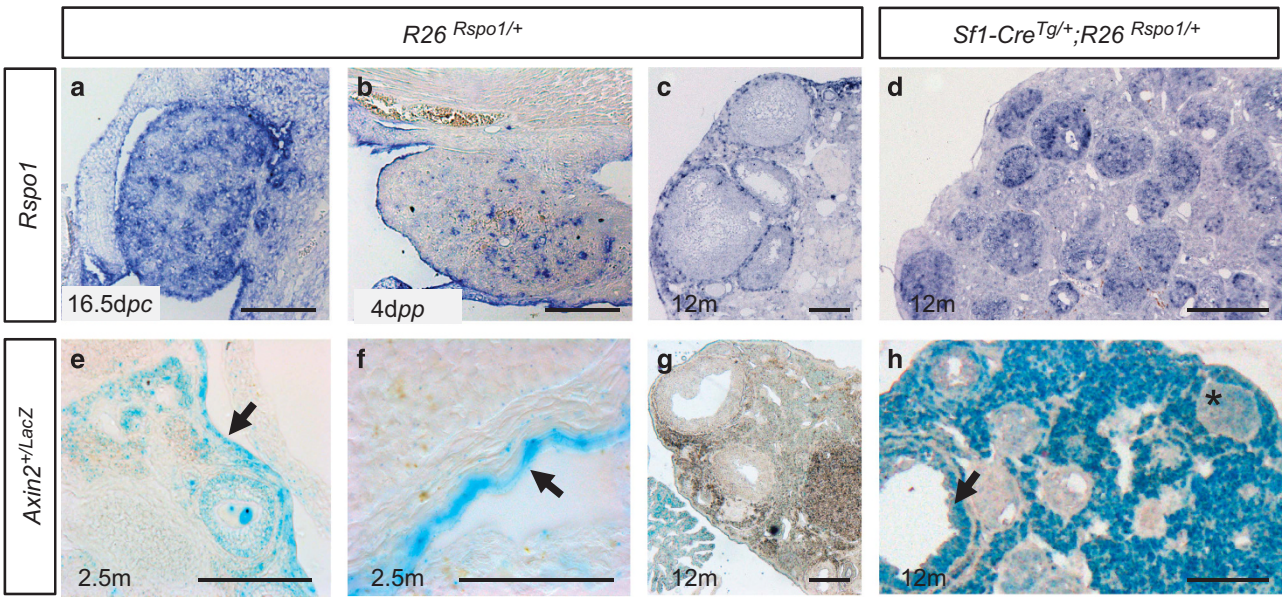

Figure 1. Pattern of *Rspo1* expression and activation of WNT signaling in ovaries. Expression of *Rspo1* revealed by *in situ* hybridization in *R26*$^{Rspo1/+}$mouse ovaries at 16.5 d*pc* (**a**), 4 d*pp* (**b**) and 12 months (**c**). *Rspo1* is expressed at low level in the *R26*$^{Rspo1/+}$mouse adult ovary, mainly in the epithelial surface and in granulosa cells of some follicles in the ovarian cortex, whereas adult *Sf1-Cre*$^{Tg/+}$; *R26*$^{Rspo1/+}$ovaries display *Rspo1* expression throughout the whole organ (**d**). Activation of the canonical WNT signaling by RSPO1 visualized by β-galactosidase staining of ovaries expressing the *Axin2-LacZ* reporter. *Axin2-LacZ* is expressed at 2.5 and 12 months in pre-antral follicles and the stroma (**e** and **g**) and strongly expressed in oocytes and the epithelial surface surrounding the ovary (**e** and **f**, arrow) in *R26*$^{Rspo1/+}$mice. Induced *Rspo1* expression leads to *Axin2-LacZ* expression in the whole *Sf1-Cre*$^{Tg/+}$; *R26*$^{Rspo1/+}$ovary (**h**) with strong staining in granulosa cells (arrow) and weaker staining in aberrant follicular structures lesions (*). Scale bars: 300 μm.

Rspo1 activation induces ovarian defects, subfertility and cancer

To evaluate the effect of RSPO1 expression on ovarian function we first assessed the fertility of *Sf1-Cre*$^{Tg/+}$; *R26*$^{Rspo1/+}$ female mice. Litter sizes were significantly reduced with only 1.25 pup/female (±1.58) compared with 7.25 pups/female (±1.16) for *R26*$^{Rspo1/+}$ littermates ($n = 8$ plugged female per genotype). By the age of 6 months double-transgenic mice were all sterile ($n = 8$). Macroscopic observation of dissected ovaries revealed a marked increase in the size of mutant ovaries when compared with those of the control littermates (Figures 2a–c). The size of the transgenic ovaries increased over time (data not shown).

To gain insides into the ovarian phenotype, we examined 170 haematoxylin and eosin-stained slides containing serial sections from 14 murine ovaries from *Sf1-Cre*$^{Tg/+}$; *R26*$^{Rspo1/+}$ mice. Histological analysis revealed a variety of abnormalities, ranging from 100% penetrance of dense follicle-like lesions to tumors in about 10% of ovaries (Figure 2). The ovarian tissue presented multifocal aggregates of neoplastic cells that arrange either in discrete solid aggregates, solid sheets or in microfollicular pattern (Figures 2f–h) reminiscent to granulosa cells. They are bland, ovoid, have distinct borders, scant amount of cytoplasm and ovoid nuclei. On the basis of these observations, we conclude that GCTs accumulate in *Sf1-Cre*$^{Tg/+}$; *R26*$^{Rspo1/+}$ mouse ovaries. None of these abnormalities were detected in control ovaries (Figure 2d). A proportion of these follicle-like structures developed into blood-filled cysts (Figures 2i and j) surrounded by cuboidal cells (Figure 2j) that were never observed in ovaries from control animals. In addition, fewer *corpora lutea* (CLs) were observed which is in agreement with the reduced fertility of the *Sf1-Cre*$^{Tg/+}$; *R26*$^{Rspo1/+}$ females (Figure 2e). A proportion of regressing CLs contained erythrocytes infiltration (Figures 2l and m). One-year-old animals carried bigger cysts (Figures 2k and n), which, in some cases, contained layered keratinocytes in the cavity (Figure 2n). In addition to the accumulation of GCT, solid tumors were observed in 12–18-month-old females with 1 tumor/13 *Sf1-Cre*$^{Tg/+}$; *R26*$^{Rspo1/+}$ and 3/19 *Sf1-Cre*$^{Tg/+}$; *R26*$^{Rspo1/Rspo1}$ females, whereas 0/22 control littermates were scored (Figure 2c). The severity of the different defects varied between animals and was not linked to whether they were heterozygous or homozygous for the *Rosa26-Rspo1* transgene.

We next analyzed whether GCTs were proliferative or undergoing apoptosis in 40 days post partum (d*pp*) *Sf1-Cre*$^{Tg/+}$; *R26*$^{Rspo1/+}$ ovaries using immunostaining for MKI67 and active CASP3, respectively, two markers of these processes. Only occasionally, we observed a cell expressing one of these markers in the GCT, implying that cell proliferation and apoptosis were negligible in these structures (Supplementary Figures S2A–D). Interestingly, increased proliferation was detected in the stromal compartment of *Sf1-Cre*$^{Tg/+}$; *R26*$^{Rspo1/+}$ ovaries (Supplementary Figures S2A and B). Consistent with this proliferative activity and clear staining for the theca cell marker SF1 (Supplementary Figures S2E and F), the theca cell layer seems to be expanded in size as indicated by SF1 staining (Supplementary Figure S2F).

We conclude that *Rspo1* acts as an oncogene in the ovary because its upregulation leads to ovarian tumor development.

Ovarian defects induced by RSPO1 expression occur from the onset of puberty

We next examined the development of the ovarian phenotype in *Sf1-Cre*$^{Tg/+}$; *R26*$^{Rspo1/+}$ mice before and soon after pubertal age. Immunostaining revealed that follicle-like structures are composed of FOXL2-positive granulosa cells (Figures 3e and f) indicating they are indeed aberrant follicles. To investigate when these abnormal follicular structures first appear, we analyzed histological sections at different stages. Pre-pubertal ovaries (21 d*pp*) appeared normal and no follicular lesions were detected (Figures 5a and b). The first phenotypic changes became apparent in 28 d*pp* ovaries ($n = 6$; Figures 3a and b). At this age most of the follicles contained an oocyte. By 40 d*pp*, serial histological sections analysis revealed an increased abundance of aberrant follicular structures with the majority of follicles being devoid of oocytes (Figures 3c and d). To further investigate the status of the aberrant follicles, we stained sections of ovaries from 40 d*pp* mice for AMH (anti-Müllerian hormone), a specific marker of early granulosa cells in primary to early antral follicles.[32] AMH-positive follicles were observed at this stage in *Sf1-Cre*$^{Tg/+}$; *R26*$^{Rspo1/+}$ mice, however, the abnormal follicular structures were negative for this marker (Figures 3g and h). Vimentin (VIM), a marker for mural granulosa cells of antral follicles, was expressed in both *R26*$^{Rspo1/+}$and *Sf1-Cre*$^{Tg/+}$; *R26*$^{Rspo1/+}$ ovaries (Figures 3i and j) and was also readily detectable in aberrant follicles (Figure 3j). Thus, GCT in *Sf1-Cre*$^{Tg/+}$; *R26*$^{Rspo1/+}$ ovaries originate from maturing antral follicles and appear around the onset of puberty, suggesting that their formation is sensitive to gonadotrophins, two specifications of adult GCT.[29]

RSPO1 expression impairs ovulation leading to the formation of GCT

As the *Sf1-Cre* transgene is also expressed in the pituitary that produces multiple hormones and especially growth hormone, we examined *Sf1-Cre*$^{Tg/+}$; *R26*$^{Rspo1/+}$ pups. Female and male mice were healthy and their body size was normal ($n = 6$; data not shown), indicating that activating *Rspo1* mutations do not hamper the development and functions of this organ. We next investigated serum levels of gonadotropins, estradiol and progesterone in adult *Sf1-Cre*$^{Tg/+}$; *R26*$^{Rspo1/+}$ females (Figure 4a). Luteinizing Hormone (LH) and progesterone levels were considerably lower in *Sf1-Cre*$^{Tg/+}$; *R26*$^{Rspo1/+}$ mice, compared with *R26*$^{Rspo1/+}$females. This observation was consistent with the low level of LH receptors observed in the ovaries (Figures 4c and e) and the lack of *corpora lutea* (Figure 2e). In contrast, follicle-stimulating hormone (FSH) levels were three times higher in *Sf1-Cre*$^{Tg/+}$; *R26*$^{Rspo1/+}$ mice (Figure 4a).

In laboratory mouse strains, puberty occurs between 30–40 d*pp*.[33] Although GCT accumulation arises at the onset of puberty, we hypothesized that gonadotropins are involved in GCT formation in *Sf1-Cre*$^{Tg/+}$; *R26*$^{Rspo1/+}$ ovaries. Thus, we stimulated follicular maturation by injecting PMSG to pre-pubertal females (21–24 d*pp*). Forty-eight hours after PMSG administration, numerous large antral follicles in both *Sf1-Cre*$^{Tg/+}$; *R26*$^{Rspo1/+}$ and *R26*$^{Rspo1/+}$ ovaries were observed (Figures 5c and d), whereas they were absent in the untreated females (Figures 5a and b). This indicates that RSPO1 does not impair follicular growth upon FSH stimulation. However, most of these large antral follicles in *Sf1-Cre*$^{Tg/+}$; *R26*$^{Rspo1/+}$mice exhibited structural abnormalities ranging from asymmetric repartition of granulosa cells to naked or abnormal oocytes (Figures 5c–g) as described in ref. 34.

In order to test whether the antral follicles present in PMSG-treated pre-pubertal *Sf1-Cre*$^{Tg/+}$; *R26*$^{Rspo1/+}$ females are competent for ovulation, superovulations were induced by injecting human chorionic gonadotropin (hCG) 48 h after PMSG administration. Ovulation takes place about 12 h post-hCG injection. We first examined the expression of *Fshr* and *Foxo1,* two factors involved in follicular development, 4 h after LH/hCG injection and found no significant differences between the two genotypes (Figure 6a). Twenty hours after hCG injection, control ovaries were mainly constituted by post-ovulatory CLs, but none or only a few were identified in *Sf1-Cre*$^{Tg/+}$; *R26*$^{Rspo1/+}$ females (Figures 6b and c). Strikingly, in *Sf1-Cre*$^{Tg/+}$; *R26*$^{Rspo1/+}$ ovaries, follicular lesions began to emerge and many large antral follicles were still apparent, some of which still contained oocytes (Figure 6c), suggesting that ovulation did not process efficiently. To confirm this observation, we quantified ovulated oocytes in superovulated females. Indeed, the number of ovulated oocytes was significantly reduced in *Sf1-Cre*$^{Tg/+}$; *R26*$^{Rspo1/+}$ females (Figure 6d) and when ovulated, the oocytes were devoid of a *cumulus oophorus* (data not shown). Moreover, we observed a dramatic reduction of the level of expression of *Amphiregulin* (*Areg*) and *Epiregulin* (*Ereg*), two EGF-like

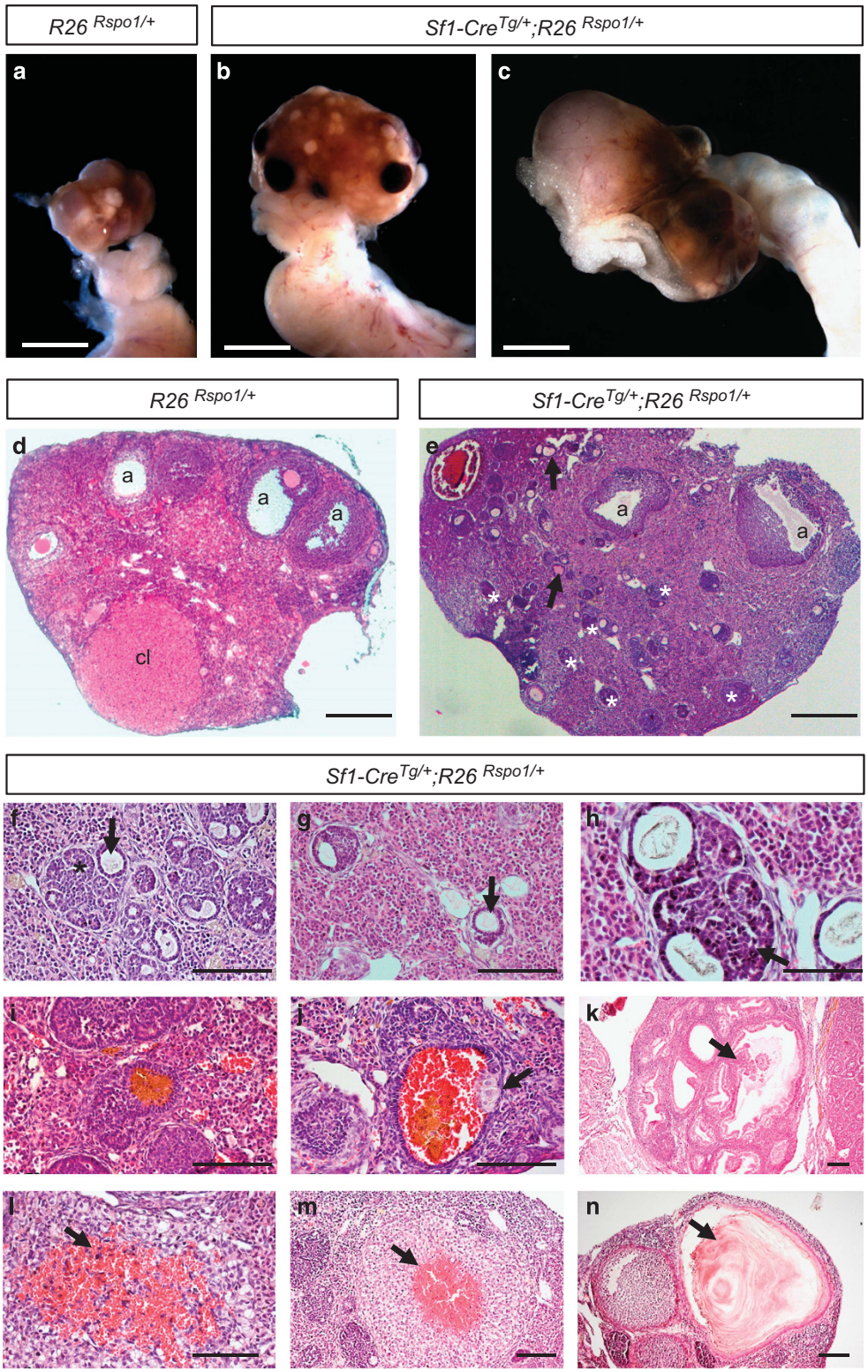

Figure 2. Ovarian defects and tumors in *Sf1-Cre*$^{Tg/+}$; *R26*$^{Rspo1/+}$ovaries. Macroscopic view of 18-month-old *R26*$^{Rspo1/+}$ (**a**) and *Sf1-Cre*$^{Tg/+}$; *R26*$^{Rspo1/+}$ovaries (**b** and **c**). The size of the *Sf1-Cre*$^{Tg/+}$; *R26*$^{Rspo1/+}$ovaries is increased in comparison with the control ovary owing to the presence of prominent tumor tissue (**c**) and/or blood-filled cysts (**b**). Magnification 10×. Histological sections (haematoxylin and eosin staining) analysis of 12-month-old ovaries. *Sf1-Cre*$^{Tg/+}$; *R26*$^{Rspo1/+}$ovaries (**e**) contain numerous multifocal aggregates of neoplastic cells that arrange either in discrete solid aggregates (*) or in microfollicular pattern (arrows) in comparison with *R26*$^{Rspo1/+}$ovaries (**d**). Scale bars, 500 μm. Magnifications of structural abnormalities in *Sf1-Cre*$^{Tg/+}$; *R26*$^{Rspo1/+}$ovaries (**f**–**n**): neoplastic cells arranged in microfollicular or rosette-like pattern (**f**; *) with central pale eosinophilic globule (Call–Exner body; **f** and **g** arrow); neoplastic cells arranged in solid sheets composed of bland, ovoid, scant amount of cytoplasm and ovoid nuclei granulosa cells. (**h**, arrow): hematocysts (**i** and **j**), with columnar cells (**j**, arrow), CL or regressing CL with erythrocytes infiltration (**l** and **m**, arrow), Ovarian epithelial cyst composed of cystic and papillary structures lined with tall columnar ciliated epithelium. (**k**, arrow) and ovarian epithelial inclusion cyst composed of keratinized squamous epithelium (**n**, arrow). Scale bars: 100 μm. a, antral follicle; cl, *corpus luteum*.

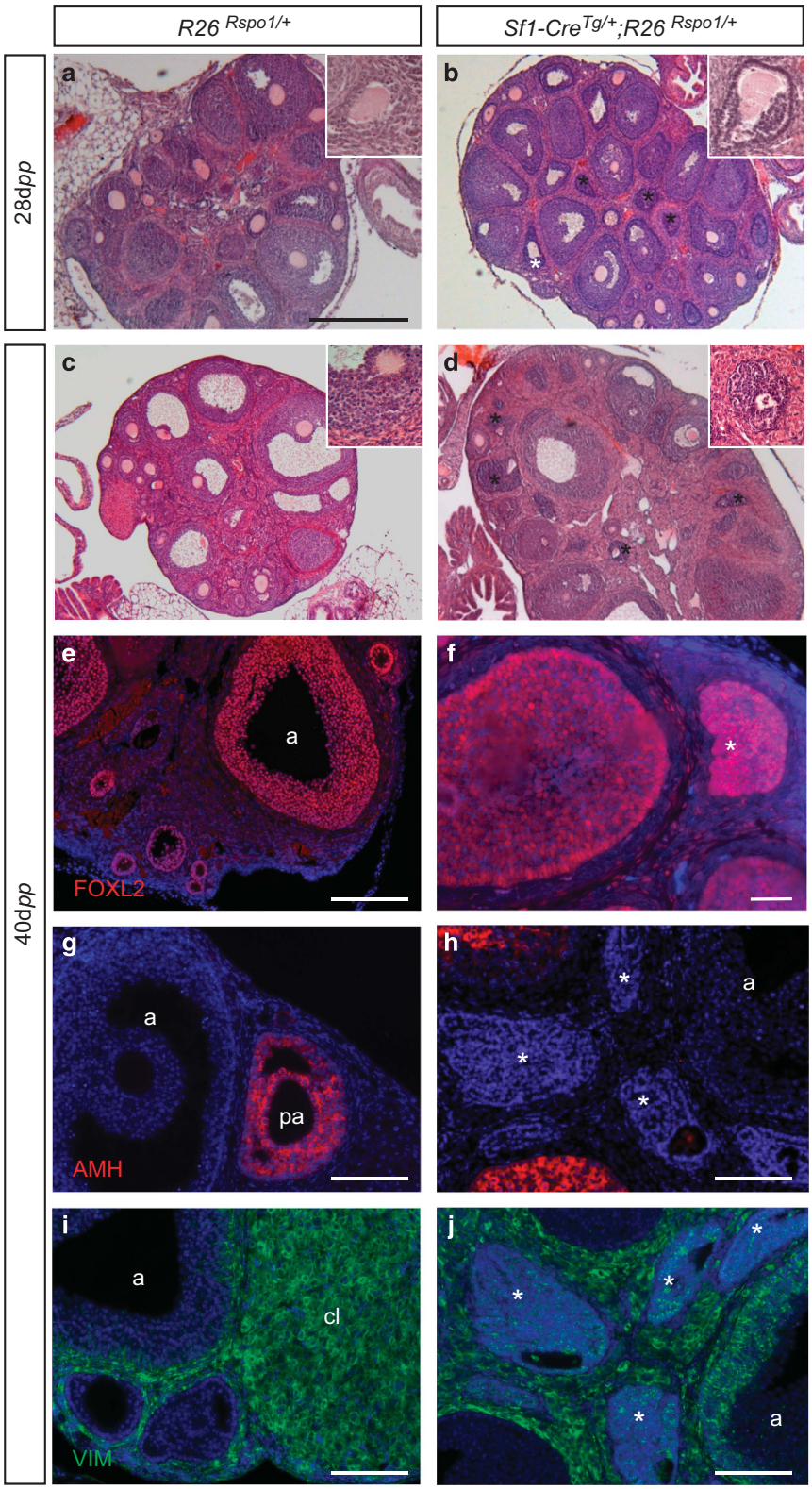

Figure 3. *RSPO1* promotes GCT. Histological analysis (haematoxylin and eosin staining) of $R26^{Rspo1/+}$ and $Sf1\text{-}Cre^{Tg/+}$; $R26^{Rspo1/+}$ ovaries at 28 d*pp* (**a** and **b**) and 40 d*pp* (**c** and **d**). Follicle-like structures (*) consisting of nests of disorganized, pleiomorphic granulosa cells become evident at 28 d*pp* (**b**) in $Sf1\text{-}Cre^{Tg/+}$; $R26^{Rspo1/+}$ ovaries, whereas they are not observed in $R26^{Rspo1/+}$ovaries (**a**). They enclose oocytes at 28 d*pp* (**b**), whereas they lack an antrum and contain no visible or a degenerating oocyte at 40 d*pp* (**d**). Scale bar: 300 μm. Immunolabelling of FOXL2 (**e** and **f**), AMH (**g** and **h**) and Vimentin (VIM) (**i** and **j**) in $R26^{Rspo1/+}$ (left panel) and $Sf1\text{-}Cre^{Tg/+}$; $R26^{Rspo1/+}$ ovaries (right panel) at 40 d*pp*. FOXL2 staining in the GCT (**f**; *) confirms the presence of granulosa cells in these follicle-like structures in $R26^{Rspo1/+}$ovaries (**e**). The absence of AMH staining (**h**) and the presence of VIM staining (**j**) in GCT (*) suggest that follicular maturation can occur up to the antral stages. Nuclei are labeled with DAPI (blue). Scale bars: 100 μm. a, antral follicle; pa, pre-antral follicle, cl, *corpus luteum*.

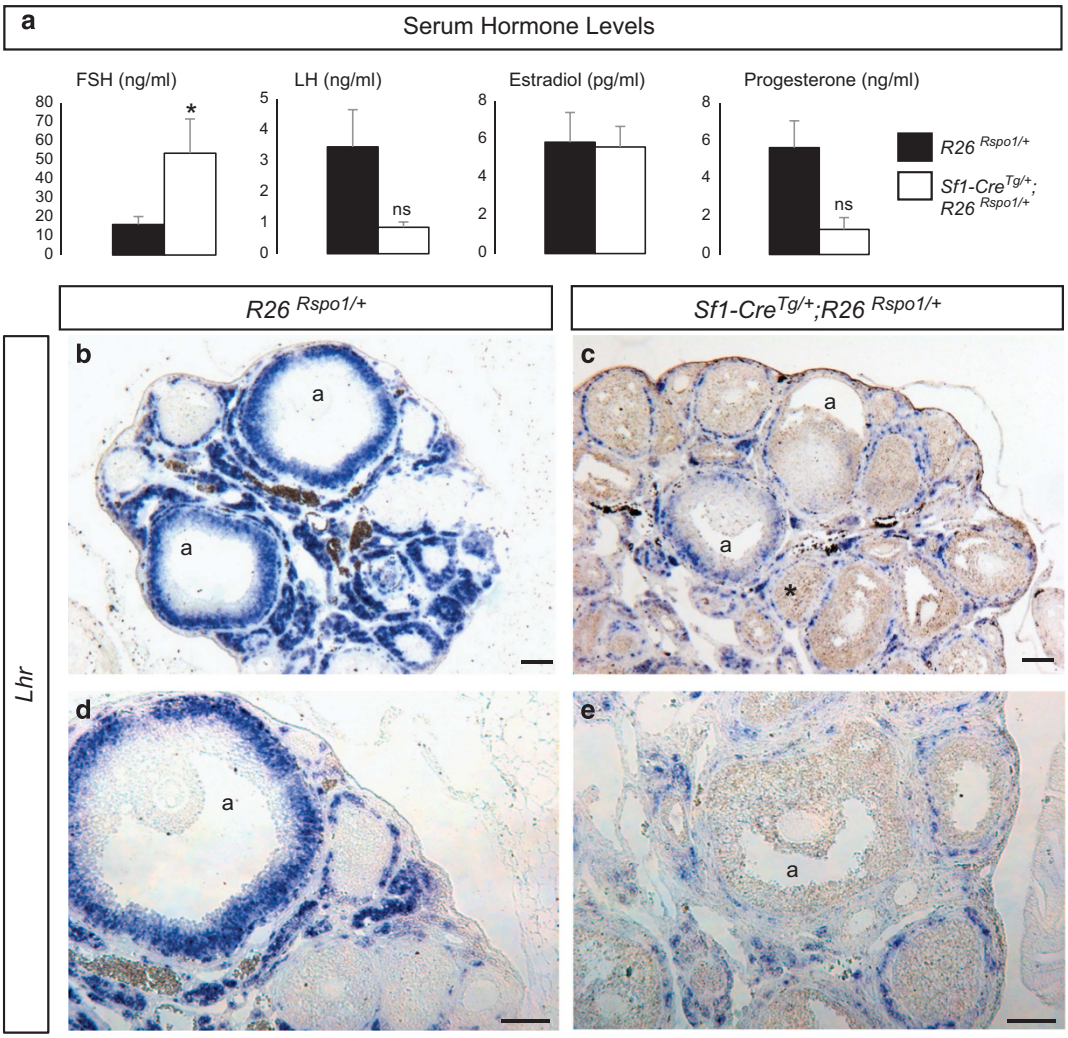

Figure 4. Induced *Rspo1* expression impairs LH-mediated luteinization. (**a**) Serum levels of FSH, LH, estradiol and progesterone in $R26^{Rspo1/+}$ (black bars) and $Sf1\text{-}Cre^{Tg/+}$; $R26^{Rspo1/+}$ ovaries (white bars) from adult females ($n = 5$ for each genotype). Bars represent mean ± s.e.m. with significance set at $P < 0.05$ (*). Expression of *LH receptor* revealed by *in situ* hybridization in adult (P40) $R26^{Rspo1/+}$and $Sf1\text{-}Cre^{Tg/+}$; $R26^{Rspo1/+}$ovaries (**b**–**e**). *Lhr* is strongly expressed in mural granulosa cells of mature antral (**a**) follicles (**b** and **d**) and in the theca cells of $R26^{Rspo1/+}$ovaries, whereas *Lhr* expression is clearly downregulated in antral follicles (**c** and **e**) of $Sf1\text{-}Cre^{Tg/+}$; $R26^{Rspo1/+}$ ovaries and is absent from GCT (*). Scale bars: 100 μm. ns, not significant.

factors involved in cumulus cell-oocyte complex expansion and thus required for ovulation (Figure 6a), which could at least partially explain the improper ovulation phenotype in $Sf1\text{-}Cre^{Tg/+}$; $R26^{Rspo1/+}$ females. The lack of CLs in $Sf1\text{-}Cre^{Tg/+}$; $R26^{Rspo1/+}$ ovaries (Figure 6c) suggests that RSPO1 expression impairs the terminal differentiation of antral follicles. Indeed, the expression of *Lhr*, *Cyp11a1* and *Star*, key genes of luteinization process of the granulosa cells which occurs upon LH/hCG surge, was significantly downregulated in $Sf1\text{-}Cre^{Tg/+}$; $R26^{Rspo1/+}$ (Figure 6a). As a result, although $R26^{Rspo1/+}$ ovaries were filled with CLs expressing CYP11A1, only few CYP11A1-positive CL were observed in $Sf1\text{-}Cre^{Tg/+}$; $R26^{Rspo1/+}$ ovaries (Figures 6f and g). Interestingly, the newly formed follicular lesions were devoid of CYP11A1 (Figure 6g). In addition, 21–24 d*pp* superovulated $Sf1\text{-}Cre^{Tg/+}$; $R26^{Rspo1/+}$ ovaries contained aberrant follicles including degenerating oocytes as observed in 40 d*pp* non-superovulated $Sf1\text{-}Cre^{Tg/+}$; $R26^{Rspo1/+}$ ovaries (Figures 3d and 6e), suggesting that follicular lesions become apparent in the later stages of follicular development.

Altogether our results demonstrate that follicular abnormalities observed in $Sf1\text{-}Cre^{Tg/+}$; $R26^{Rspo1/+}$ ovaries are driven by puberty, that $Sf1\text{-}Cre^{Tg/+}$; $R26^{Rspo1/+}$ ovaries are unable to properly respond to LH and that GCT formation is linked to FSH stimulation. These results show that superovulation experiments induce and accelerate the formation of GCT and that *Rspo1* downregulation within adult ovary is required for the proper occurrence of the ovulation process and the subsequent formation of CLs.

Induced expression of RSPO1 promotes cell junction adherence and epithelial traits in GCT

Next, we searched for an explanation for the persistence of these abnormal follicular structures. RSPO1 is typically associated with canonical WNT signaling as corroborated by the expression of the $Axin2^{+/LacZ}$reporter[31] (Figures 1g and h). However, CTNNB1 is also a component of adherens junctions, where it associates with cadherins (CDH).[8,35] Maintaining adherence junctions has been shown previously to inhibit apoptosis of granulosa cells thus preventing follicular degeneration.[36] Therefore, the presence of adherens junctions was investigated in ovaries of 6-month-old $Sf1\text{-}Cre^{Tg/+}$; $R26^{Rspo1/+}$ and $R26^{Rspo1/+}$ mice by immunostainings using the markers CTNNB1 and cell-adhesion molecule N-cadherin (CDH2). CTNNB1 was mostly detected at the membrane of granulosa cells of pre-antral follicles and in granulosa cells surrounding the antrum in larger antral follicles in control ovaries (Figures 7a and c). CTNNB1 was enriched at the membrane of the cells in the GCT in $Sf1\text{-}Cre^{Tg/+}$; $R26^{Rspo1/+}$ ovaries

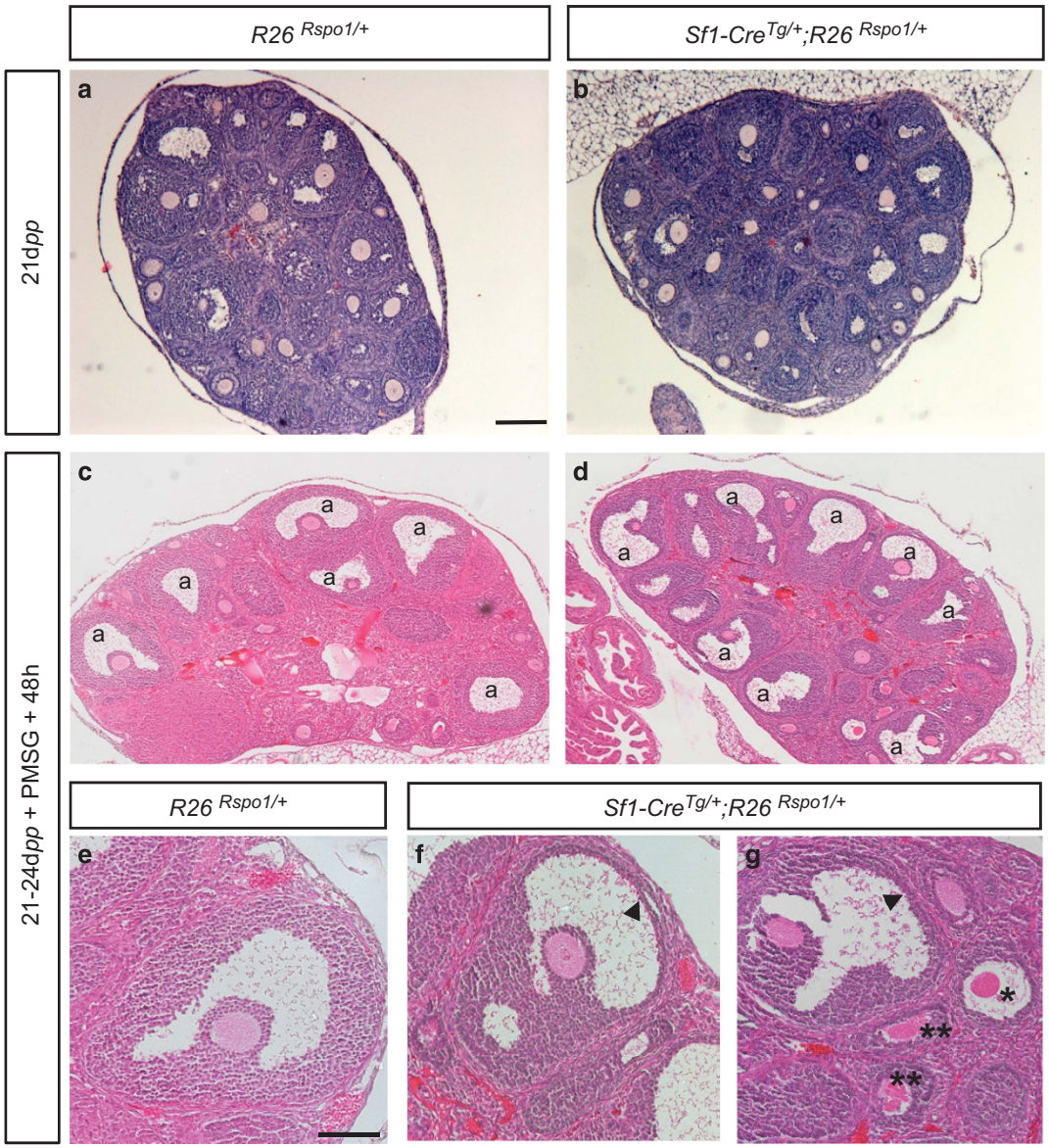

Figure 5. *Sf1-Cre*$^{Tg/+}$; *R26*$^{Rspo1/+}$ ovaries respond to hormonal stimulation. Histological analysis (haematoxylin and eosin staining) of *R26*$^{Rspo1/+}$ (**a**, **c** and **e**) and *Sf1-Cre*$^{Tg/+}$; *R26*$^{Rspo1/+}$ (**b**, **d**, **f** and **g**) ovaries of 21 d*pp* (**a** and **b**) and at 21–24 d*pp* stimulated by PMSG injection and collected 48 h later (**c**–**g**). When stimulated by PMSG, ovaries from both genotypes contain large antral (**a**) follicles (**c** and **d**) but in *Sf1-Cre*$^{Tg/+}$; *R26*$^{Rspo1/+}$ mice, most of these follicles exhibit dissymmetric mural granulosa (**f** and **g**, arrowheads) when compared with follicles of *R26*$^{Rspo1/+}$ ovaries (**e**). Aberrant follicles are also observed containing naked (*) or degenerating (**) oocytes (**g**). Scale bar: 300 μm (**a**–**d**) and 100 μm (**e**–**g**).

(Figures 7b and d). The presence of CDH2 was evident at all stages during maturation in both genotypes (Supplementary Figures S3A, B). GCT also strongly expressed membrane-bound plakoglobin (JUP), a component of desmosomes and intermediate junctions (Figures 7e and f), and the epithelial markers KRT18 and pan-cytokeratin (Figures 7g and h and Supplementary Figures S3C–F) that are absent or weakly expressed in follicles in control ovaries. These data reveal the presence of strong intercellular junctions in GCT in *Sf1-Cre*$^{Tg/+}$; *R26*$^{Rspo1/+}$ ovaries, indicating that induced expression of *Rspo1* increases cellular adhesion, which in turn may promote epithelialisation of granulosa cells and the persistence of the follicular remnants.

DISCUSSION

Although RSPO1 is crucial for ovarian development,[14] here we show that its postnatal downregulation is critical for the maintenance of a healthy adult ovary. When RSPO1 expression is maintained, GCT appear at the onset of puberty in 100% of the cases. Prolonged RSPO1 expression allows follicular maturation until the late antral stage. Most follicles are capable of responding to FSH stimulation as previously reported for induced CTNNB1 expression,[37] and fail to respond to LH. It has been shown that FSH increases the occurrence and onset of GCT formation.[38] These GCT are classified as adult GCT.[29] Accordingly, we observed high FSH levels that could contribute to the adult GCT formation in *Sf1-Cre*$^{Tg/+}$; *R26*$^{Rspo1/+}$ mice.

Endocrine functionality of CL involves LGR receptors.[25,26] However, neither *Rspo1* nor the CTNNB1 target *Axin2* is expressed in these structures, which suggests that LGRs may act through an RSPO1/CTNNB1 independent pathway in this cell type. In contrast, RSPO1, stabilized CTNNB1 and LGR5 are expressed in the OSE stem cells that contribute to post-ovulatory repair,[24] putting forward that these factors act together in the ovulation process. However, the ovulatory defects observed in our model prevented us from analyzing whether induced *Rspo1* affects CL physiology and post-ovulatory OSE repair.

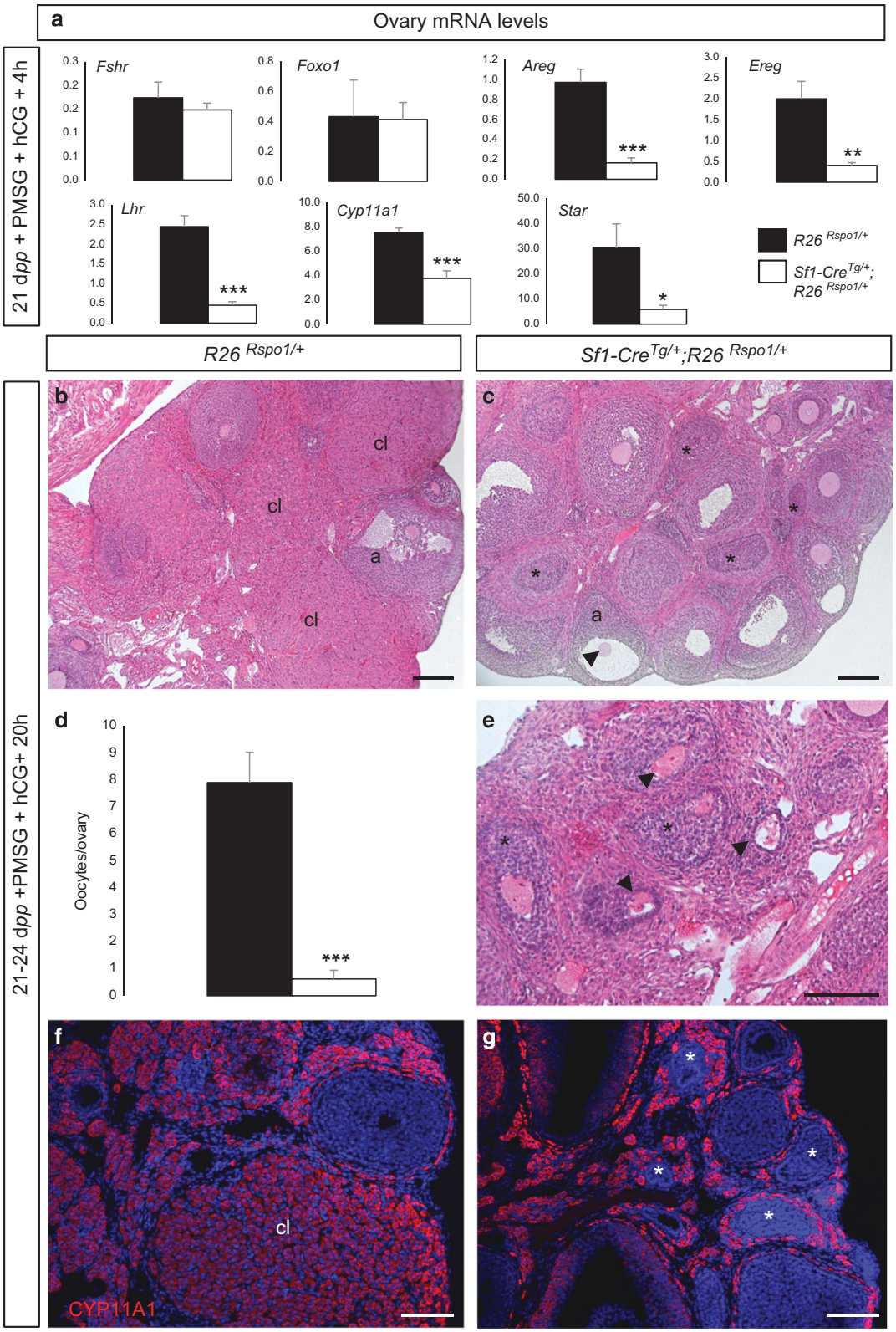

Figure 6. Induced *Rspo1* expression prevents ovulation. Quantitative RT–PCR analysis of *Fshr*, *Foxo1*, *Areg*, *Ereg*, *Lhr*, *Cyp11a1* and *Star* expression in $R26^{Rspo1/+}$ (black bars) and $Sf1\text{-}Cre^{Tg/+}$; $R26^{Rspo1/+}$ ovaries (white bars) from 21–24 d*pp* superovulated mice, using *Sdha1* as the normalization control (**a**). Bars represent mean ± s.e.m. ($n = 6$ for each genotype) with significance set at $P < 0.05$ (*), $P < 0.01$ (**) and $P < 0.001$ (***). Histological analysis (haematoxylin and eosin staining) of $R26^{Rspo1/+}$ and $Sf1\text{-}Cre^{Tg/+}$; $R26^{Rspo1/+}$ ovaries at 21–24 d*pp* stimulated by hCG (**b**, **c** and **e**). $R26^{Rspo1/+}$ ovaries (**b**) contain many *corpora lutea* (cl) which are rarely observed in $Sf1\text{-}Cre^{Tg/+}$; $R26^{Rspo1/+}$ ovaries (**c**). Instead, these ovaries display several GCT (*) and naked oocytes (arrowhead) in antral (indicated as a) follicles (**c**) and degenerating follicles (arrowhead) (**e**). Superovulation experiments show a reduced number of ovulated oocytes (**d**) with an average of 8 and 0.6 oocyte/ovary ($n = 8$–10) in $R26^{Rspo1/+}$ and $Sf1\text{-}Cre^{Tg/+}$; $R26^{Rspo1/+}$ females, respectively. CYP11A1 revealed by immunostaining is highly expressed in CL of $R26^{Rspo1/+}$ ovaries (**f**) but absent in the abnormal follicles (*) of $Sf1\text{-}Cre^{Tg/+}$; $R26^{Rspo1/+}$ ovaries (**g**). Nuclei are labeled with DAPI (blue). Scale bars: 100 μm.

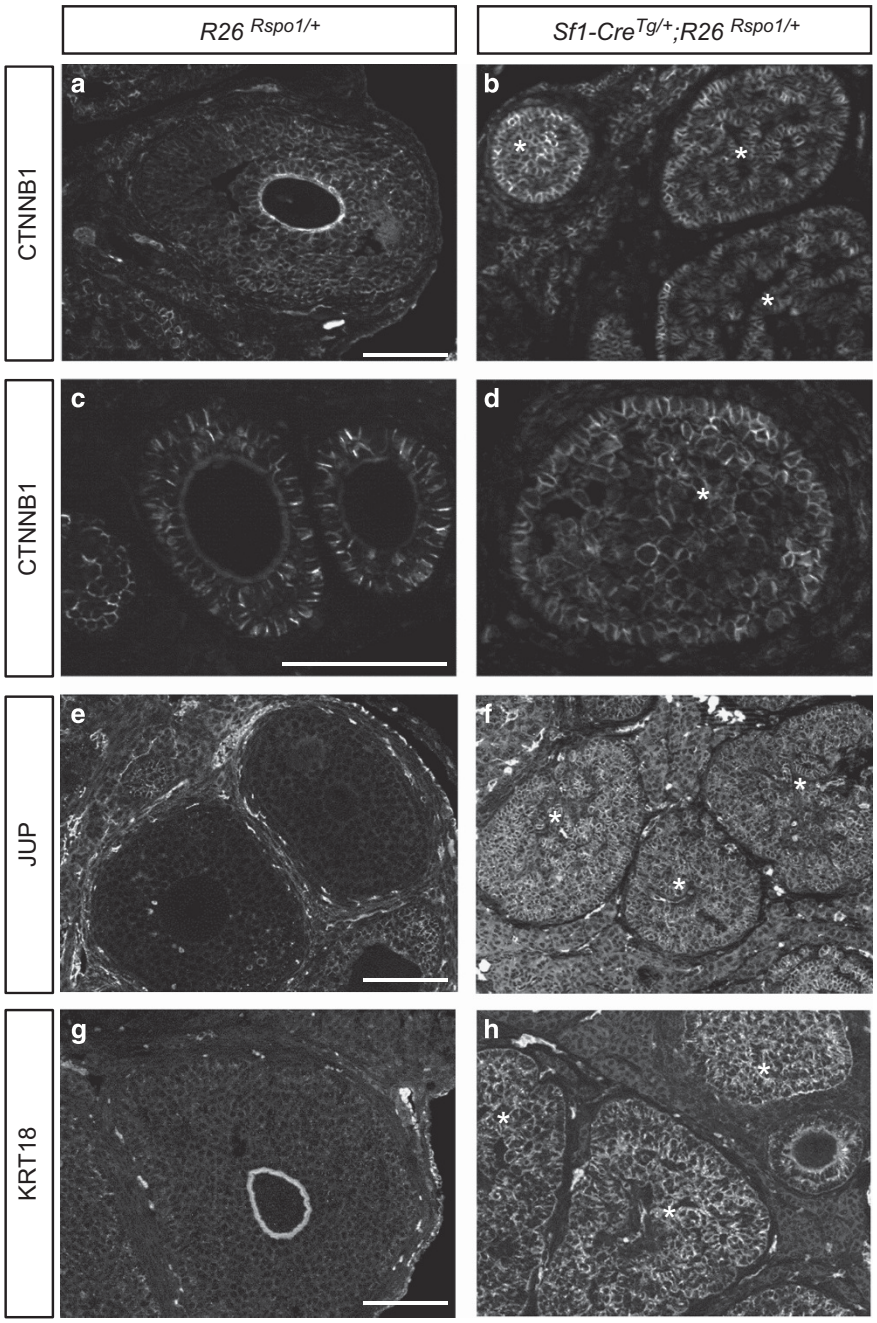

Figure 7. RSPO1 expression maintains intercellular junctions and epithelial identity in GCT. Immunostaining for CTNNB1 (**a**–**d**), JUP (**e** and **f**), and KRT18 (**g** and **h**) in 6-month-old *R26*$^{Rspo1/+}$ (left panel) and *Sf1-Cre*$^{Tg/+}$; *R26*$^{Rspo1/+}$ (right panel) ovaries. Membrane staining for CTNNB1 and JUP underline cellular junctions in these follicle-like structures (**h**). Nuclei are labeled with DAPI (blue). Scale bars: 100 μm.

In addition to the granulosa cell phenotype, we observed an enriched population of SF1-positive theca cells suggesting a role of CTNNB1 signaling in differentiation of steroidogenic lineages. The steroidogenic precursors of adrenal and gonadal cells have a common origin[39] and both arise from a pool of WT1-positive cells.[40,41] In adrenals, CTNNB1 is required for the formation and maintenance of the steroidogenic cells of the adrenal cortex,[42,43] but the role of this signaling pathway in the fate of the theca cells has not been investigated to date.

Ablation of *Rspo1* induces a precocious differentiation of granulosa cells during fetal development.[20] This demonstrates that *Rspo1* is required to maintain an undifferentiated state of the granulosa cell progenitors during early development, before *Rspo1* expression decreases within the ovary around birth. Here, we show that when *Rspo1* expression is maintained, it alters the differentiation of granulosa cells via their epithelialization. First, CTNNB1 and JUP are maintained at the plasma membrane of aberrant follicular structures and contribute to cell junction formation. Although follicular atresia is promoted by oocytes disruption,[34] the maintenance of intercellular junctions can prevent degeneration of the granulosa cells.[35] This suggests that stabilization of cell–cell contacts promote survival of the GCT in *Sf1-Cre*$^{Tg/+}$; *R26*$^{Rspo1/+}$mice. Interestingly, in a granulosa cell dominant-stable CTNNB1 mutant mouse model, GCTs develop via a mechanism that mainly implies canonical WNT signaling.[44] Here, we show that RSPO1 activation in adult ovaries induces formation of GCTs by regulating not only canonical WNT signaling activation but also intercellular junction homeostasis in granulosa cells.

Second, GCT exhibit not only granulosa cell identity as highlighted by FOXL2 and Vimentin expression, but also epithelial cell traits are reactivated as shown by the concomitant expression of epithelial markers like pan-cytokeratin and KRT18. Granulosa cells originate from surface epithelial progenitors.[45] Our results suggest that adult granulosa cells maintain the potential to reactivate their epithelial program if properly stimulated, and that RSPO1 is sufficient to induce this program. Moreover, FOXO1/3 and PTEN factors mutations in granulosa cells also promoted epithelial traits reactivation in GCTs.[38]

The mixed identity of GCT as granulosa cells and epithelial progenitors is likely a susceptibility factor for ovarian pathologies including ovarian cancers. Indeed, our results evidence that afterbirth maintenance of RSPO1 expression induces GCT but also severe ovarian pathologies and eventually cancers in mice. In human RSPO1 has been reported as a susceptibility factor of ovarian epithelial cancers and is amplified in 8% of them,[3,4] but so far its exact role in ovarian cancers was not clear. Here, we show for the first time that the overexpression of RSPO1 in mouse ovarian tissues is sufficient to lead to GCT formation with 100% penetrance. Our results highlight RSPO1 as a main player in the ovarian oncogenic process and provide new insights into the molecular roles of RSPO1 in the pathology.

MATERIALS AND METHODS

Mouse strains and genotyping

The experiments were carried out in compliance with the relevant institutional and French animal welfare laws, guidelines and policies and have been approved by the French ethics committee (CIEPAL: NCE/2011-12).

Rspo1 gain-of-function model (Supplementary Figure S1) carries an inducible *Rspo1* gene knocked into the *Rosa26* locus. The construct is similar to the one reported in ref. 46 with the exception of the promoter. Here, the *Rosa26* promoter controls *Rspo1 expression*. $R26^{Rspo1/+}$ mice were mated with the *Sf1-Cre*^{high} ($Sf1\text{-}Cre^{Tg/+}$) strain, which drives expression of the Cre recombinase in somatic cells of the gonad from 11.5 d*pc* onward.[47] *Axin2-LacZ* mice were described previously,[31] and crossed with $Sf1\text{-}Cre^{Tg/+}$; $R26^{Rspo1/+}$ males to generate $Sf1\text{-}Cre^{Tg/+}$; $R26^{Rspo1/+}$; $Axin2^{+/LacZ}$ animals. Fertility tests were performed using 3–4-month-old $Sf1\text{-}Cre^{Tg/+}$; $R26^{Rspo1/+}$ females mated with $R26^{Rspo1/+}$ males (Supplementary Figure S1). Genotyping was performed using DNA extracted from tail tips or ear biopsies of mice. The presence of the Y chromosome and the *Axin2-LacZ* transgene was determined as described previously.[14]

Histological analysis

Ovaries were dissected, fixed in Bouin's solution overnight, and embedded in paraffin. Five-micrometer-thick sections were stained with hematoxylin and eosin. To determine the ovarian phenotype in *Rspo1* expressing ovaries, consecutive sections were analyzed. Pictures were taken with an Axioscope 2 (Zeiss, Oberkochen, Germany) or MZ9.5 (Leica, Mannheim, Germany) microscope coupled with an Axiocam MRc5 (Zeiss) or DHC490 (Leica) camera and Axiovision 4.8 (Zeiss) or application suite V3.3.0 (Leica) software, and processed with Adobe Photoshop (San Jose, CA, USA).

Serum collection and hormone assays

Blood was collected from adult mice in the same stage of estrous cycle and allowed to clot for 90 min at room temperature. Samples were then centrifuged and the serum was collected and stored at − 20 °C. Hormone analyses were performed by the Ligand Assay and Analysis Core Laboratory at The Center for Research and Reproduction, University of Virginia (Charlottesville, VA, USA). LH, FSH, estradiol and progesterone measurements were run in duplicates using specific assays ($n = 5$ for each genotype).

Superovulations

Immature 3–4-week-old mice were injected intraperitoneally (i.p.) with 5 IU/mouse pregnant mare serum gonadotropin (PMSG) (Sigma-Aldrich, St Louis, MO, USA) to promote follicle maturation, followed by 5 IU/mouse hCG (Sigma-Aldrich) 48 h later to induce ovulation. Mice were humanely killed 48 h after the first hormone injection for follicle maturation studies or 4 h and 20 h after the second injection for ovulation and luteinization studies. Ovaries, including fat pad, oviduct and partial uterine tube, were fixed in 4% paraformaldehyde or Bouin's solution overnight. For qPCR analyses, ovaries were carefully isolated from the genital tract and quickly frozen in liquid nitrogen. For oocyte counting, immature females ($n = 8$ ($R26^{Rspo1/+}$) and 10 ($Sf1\text{-}Cre^{Tg/+}$; $R26^{Rspo1/+}$) ovaries) were similarly superovulated and killed 20 h after the hCG injection. Oviducts were isolated from ovary and uterus and opened to collect the oocytes.

X-gal staining and immunological analyses

Tissue samples were fixed in 4% paraformaldehyde overnight and then processed for paraffin embedding or equilibrated in sucrose and embedded in Cryomount (Histolab, Göteburg, Sweden) for cryosectioning. Cryostat or microtome sections of 10 µm and 5 µm thickness respectively were processed for X-Gal and immunostaining. Samples for X-Gal staining were processed as described previously.[14]

Immunohistochemical experiments were performed as described in.[14] The following dilutions of primary antibodies were used: AMH (C-20, cat sc6886, Santa Cruz Biotechnology, Dallas, TX, USA) 1:200, CTNNB1 (cat 610153, BD Biosciences, San Jose, CA, USA) 1:250, active CASP3 (cat AF835, R&D Systems) 1:200, CDH2 (cat 33-3900, Invitrogen) 1:200, CYP11A1[48] 1:300, FOXL2[21] 1:400, JUP (cat 610254, BD Biosciences) 1:250, KRT18 (cat ab52948, Abcam, Cambridge, UK) 1:300, LHR (LHR-29, ATCC-CRL-2685, ATCC) 1:150, MKi67 (clone SP6, cat 9106, Thermo Fisher Scientific, Waltham, MA, USA) 1:200, SF1 (kindly provided by Professor Morohashi) 1:1000 and Vimentin (cat ab92547, Abcam) 1:200. Slides were counterstained with DAPI diluted in the mounting medium at 10 µg/ml (Vectashield, Vector laboratories, Burlingame, CA, USA) to detect nuclei. Imaging was performed with a motorized Axio ImagerZ1 microscope (Zeiss) coupled with an Axiocam Mrm camera (Zeiss) and processed with Axiovision LE (Zeiss) and Adobe Photoshop.

In situ hybridization

Tissue samples were fixed in 4% paraformaldehyde in 1 × PBS overnight at 4 °C. Seven-micrometer sections were cut for *in situ* hybridization experiments using *Rspo1* and *Lhr* digoxigenin-labeled riboprobes as described previously.[14] Each experiment was repeated on at least two gonads. Post-hybridization washes were done in 100 mM maleic acid Ph7.5, 150 mM NaCl, 0.1% (v/v) tween-20 (MABT). Imaging was performed on a MZ9.5 microscope (Leica) as described above and processed with Adobe Photoshop.

Quantitative PCR analysis

Individual ovaries from either adult or 21–24 d*pp* superovulated mice were dissected in 1 × PBS and quickly frozen in liquid nitrogen. RNA was extracted using the RNeasy Qiagen kit and reverse transcribed using the RNA RT–PCR kit (Stratagene). Primers and probes were designed by Roche Assay Design Center (http://qpcr.probefinder.com/organism.jsp). Primer sequences are available upon request to the authors. All real-time PCR assays were carried out using LightCycler Taqman Master kit (Roche, Basel, Switzerland). QPCR was performed on cDNA from one gonad and compared with a standard curve. Relative expression levels of each gene was determined in the same run and normalized on the levels of endogenous *Sdha1* cDNA. QPCR were repeated at least twice. For adult mice, $n = 4$ ($R26^{Rspo1/+}$) and 8 ($Sf1\text{-}Cre^{Tg/+}$; $R26^{Rspo1/+}$) gonads. For 21–24 d*pp* superovulated mice, $n = 6$ gonads for each genotype.

Statistical analysis

Data are shown as mean ± s.e.m.

All the data were analyzed by unpaired one-sided Student's *t*-test using Microsoft Excel (Redmond, WA, USA). Asterisks highlight the pertinent comparisons and indicate levels of significance: $*P < 0.05$, $**P < 0.01$ and $***P < 0.001$.

CONFLICT OF INTEREST

The authors declare no conflict of interest.

ACKNOWLEDGEMENTS

We thank Mireille Cutajar-Bossert for her work and management of funding and also Fariba Jianmotamedi, Aurélie Charlet and Béatrice Polo for their punctual help in this work. We are thankful to Walter Birchmeier (Berlin, Germany) for the $Axin2^{+/LacZ}$ mice and Ken Morohashi (Fukuoka, Japan) for the SF1 antibody. We thank Aitana Perea-

Gomez for critical reading of the manuscript. This work was supported by grants from the Fondation ARC pour la Recherche sur le Cancer (PJA 20131200236) and Agence Nationale de la Recherche (ANR-09-GENM-009-03 and ANR-11-LABX-0028-01). EP was supported by a fellowship from INRA and Ligue Nationale contre le Cancer.

REFERENCES

1 Clevers H, Nusse R. Wnt/beta-catenin signaling and disease. *Cell* 2012; **149**: 1192–1205.
2 Seshagiri S, Stawiski EW, Durinck S, Modrusan Z, Storm EE, Conboy CB *et al.* Recurrent R-spondin fusions in colon cancer. *Nature* 2012; **488**: 660–664.
3 Kuchenbaecker KB, Ramus SJ, Tyrer J, Lee A, Shen HC, Beesley J *et al.* Identification of six new susceptibility loci for invasive epithelial ovarian cancer. *Nat Genet* 2015; **47**: 164–171.
4 Gao J, Aksoy BA, Dogrusoz U, Dresdner G, Gross B, Sumer SO *et al.* Integrative analysis of complex cancer genomics and clinical profiles using the cBioPortal. *Sci Signal* 2013; **6**: pl1.
5 Kim KA, Kakitani M, Zhao J, Oshima T, Tang T, Binnerts M *et al.* Mitogenic influence of human R-spondin1 on the intestinal epithelium. *Science* 2005; **309**: 1256–1259.
6 Parma P, Radi O, Vidal V, Chaboissier MC, Dellambra E, Valentini S *et al.* R-spondin1 is essential in sex determination, skin differentiation and malignancy. *Nat Genet* 2006; **38**: 1304–1309.
7 de Lau W, Peng WC, Gros P, Clevers H. The R-spondin/Lgr5/Rnf43 module: regulator of Wnt signal strength. *Genes Dev* 2014; **28**: 305–316.
8 Kemler R. From cadherins to catenins: cytoplasmic protein interactions and regulation of cell adhesion. *Trends Genet* 1993; **9**: 317–321.
9 Lyashenko N, Winter M, Migliorini D, Biechele T, Moon RT, Hartmann C *et al.* Differential requirement for the dual functions of beta-catenin in embryonic stem cell self-renewal and germ layer formation. *Nat Cell Biol* 2011; **13**: 753–761.
10 Maeda O, Usami N, Kondo M, Takahashi M, Goto H, Shimokata K *et al.* Plakoglobin (gamma-catenin) has TCF/LEF family-dependent transcriptional activity in beta-catenin-deficient cell line. *Oncogene* 2004; **23**: 964–972.
11 Chidgey M, Dawson C. Desmosomes: a role in cancer? *Br J Cancer* 2007; **96**: 1783–1787.
12 Tomaselli S, Megiorni F, De Bernardo C, Felici A, Marrocco G, Maggiulli G *et al.* Syndromic true hermaphroditism due to an R-spondin1 (RSPO1) homozygous mutation. *Hum Mutat* 2008; **29**: 220–226.
13 Maatouk DM, DiNapoli L, Alvers A, Parker KL, Taketo MM, Capel B *et al.* Stabilization of beta-catenin in XY gonads causes male-to-female sex-reversal. *Hum Mol Genet* 2008; **17**: 2949–2955.
14 Chassot AA, Ranc F, Gregoire EP, Roepers-Gajadien HL, Taketo MM, Camerino G *et al.* Activation of beta-catenin signaling by Rspo1 controls differentiation of the mammalian ovary. *Hum Mol Genet* 2008; **17**: 1264–1277.
15 Tomizuka K, Horikoshi K, Kitada R, Sugawara Y, Iba Y, Kojima A *et al.* R-spondin1 plays an essential role in ovarian development through positively regulating Wnt-4 signaling. *Hum Mol Genet* 2008; **17**: 1278–1291.
16 Karl J, Capel B. Sertoli cells of the mouse testis originate from the coelomic epithelium. *Dev Biol* 1998; **203**: 323–333.
17 Chassot AA, Bradford ST, Auguste A, Gregoire EP, Pailhoux E, de Rooij DG *et al.* WNT4 and RSPO1 together are required for cell proliferation in the early mouse gonad. *Development* 2012; **139**: 4461–4472.
18 Mork L, Maatouk DM, McMahon JA, Guo JJ, Zhang P, McMahon AP *et al.* Temporal differences in granulosa cell specification in the ovary reflect distinct follicle fates in mice. *Biol Reprod* 2012; **86**: 37.
19 Zheng W, Zhang H, Gorre N, Risal S, Shen Y, Liu K *et al.* Two classes of ovarian primordial follicles exhibit distinct developmental dynamics and physiological functions. *Hum Mol Genet* 2014; **23**: 920–928.
20 Maatouk DM, Mork L, Chassot AA, Chaboissier MC, Capel B. Disruption of mitotic arrest precedes precocious differentiation and transdifferentiation of pregranulosa cells in the perinatal Wnt4 mutant ovary. *Dev Biol* 2013; **383**: 295–306.
21 Rastetter RH, Bernard P, Palmer JS, Chassot AA, Chen H, Western PS *et al.* Marker genes identify three somatic cell types in the fetal mouse ovary. *Dev Biol* 2014; **394**: 242–252.
22 Auguste A, Chassot AA, Grégoire EP, Renault L, Pannetier M, Treier M *et al.* Loss of R-spondin1 and Foxl2 amplifies female-to-male sex reversal in XX mice. *Sex Dev* 2011; **5**: 304–317.
23 Hirshfield AN. Overview of ovarian follicular development: considerations for the toxicologist. *Environ Mol Mutagen* 1997; **29**: 10–15.
24 Ng A, Tan S, Singh G, Rizk P, Swathi Y, Tan TZ *et al.* Lgr5 marks stem/progenitor cells in ovary and tubal epithelia. *Nat Cell Biol* 2014; **16**: 745–757.
25 Pan H, Cui H, Liu S, Qian Y, Wu H, Li L *et al.* Lgr4 gene regulates corpus luteum maturation through modulation of the WNT-mediated EGFR-ERK signaling pathway. *Endocrinology* 2014; **155**: 3624–3637.
26 Sun X, Terakawa J, Clevers H, Barker N, Daikoku T, Dey SK *et al.* Ovarian LGR5 is critical for successful pregnancy. *Faseb J* 2014; **28**: 2380–2389.
27 Boerboom D, Paquet M, Hsieh M, Liu J, Jamin SP, Behringer RR *et al.* Misregulated Wnt/beta-catenin signaling leads to ovarian granulosa cell tumor development. *Cancer Res* 2005; **65**: 9206–9215.
28 Mullany LK, Richards JS. Minireview: Animal Models and Mechanisms of Ovarian Cancer Development. *Endocrinology* 2012; **153**: 1585–1592.
29 Jamieson S, Fuller PJ. Molecular pathogenesis of granulosa cell tumors of the ovary. *Endocr Rev* 2012; **33**: 109–144.
30 Tomaselli S, Megiorni F, Lin L, Mazzilli MC, Gerrelli D, Majore S *et al.* Human RSPO1/R-spondin1 is expressed during early ovary development and augments beta-catenin signaling. *PLoS ONE* 2011; **6**: e16366.
31 Lustig B, Jerchow B, Sachs M, Weiler S, Pietsch T, Karsten U *et al.* Negative feedback loop of Wnt signaling through upregulation of conductin/axin2 in colorectal and liver tumors. *Mol Cell Biol* 2002; **22**: 1184–1193.
32 Durlinger AL, Visser JA, Themmen AP. Regulation of ovarian function: the role of anti-Mullerian hormone. *Reproduction* 2002; **124**: 601–609.
33 Ahima RS, Dushay J, Flier SN, Prabakaran D, Flier JS. Leptin accelerates the onset of puberty in normal female mice. *J Clin Invest* 1997; **99**: 391–395.
34 Osman P. Rate and course of atresia during follicular development in the adult cyclic rat. *J Reprod Fertil* 1985; **73**: 261–270.
35 Rowlands TM, Symonds JM, Farookhi R, Blaschuk OW. Cadherins: crucial regulators of structure and function in reproductive tissues. *Rev Reprod* 2000; **5**: 53–61.
36 Makrigiannakis A, Coukos G, Christofidou-Solomidou M, Gour BJ, Radice GL, Blaschuk O *et al.* N-cadherin-mediated human granulosa cell adhesion prevents apoptosis: a role in follicular atresia and luteolysis? *Am J Pathol* 1999; **154**: 1391–1406.
37 Fan HY, O'Connor A, Shitanaka M, Shimada M, Liu Z, Richards JS *et al.* Beta-catenin (CTNNB1) promotes preovulatory follicular development but represses LH-mediated ovulation and luteinization. *Mol Endocrinol* 2010; **24**: 1529–1542.
38 Liu Z, Ren YA, Pangas SA, Adams J, Zhou W, Castrillon DH *et al.* FOXO1/3 and PTEN Depletion in Granulosa Cells Promotes Ovarian Granulosa Cell Tumor Development. *Mol Endocrinol* 2015; **29**: 1006–1024.
39 Hatano O, Takakusu A, Nomura M, Morohashi K. Identical origin of adrenal cortex and gonad revealed by expression profiles of Ad4BP/SF-1. *Genes Cells* 1996; **1**: 663–671.
40 Bandiera R, Vidal VP, Motamedi FJ, Clarkson M, Sahut-Barnola I, von Gise A *et al.* WT1 maintains adrenal-gonadal primordium identity and marks a population of AGP-like progenitors within the adrenal gland. *Dev Cell* 2013; **27**: 5–18.
41 Liu C, Peng J, Matzuk MM, Yao HH. Lineage specification of ovarian theca cells requires multicellular interactions via oocyte and granulosa cells. *Nat Commun* 2015; **6**: . 6934.
42 Kim AC, Reuter AL, Zubair M, Else T, Serecky K, Bingham NC *et al.* Targeted disruption of beta-catenin in Sf1-expressing cells impairs development and maintenance of the adrenal cortex. *Development* 2008; **135**: 2593–2602.
43 Huang CC, Miyagawa S, Matsumaru D, Parker KL, Yao HH. Progenitor cell expansion and organ size of mouse adrenal is regulated by sonic hedgehog. *Endocrinology* 2010; **151**: 1119–1128.
44 Boerboom D, White LD, Dalle S, Courty J, Richards JS. Dominant-stable beta-catenin expression causes cell fate alterations and Wnt signaling antagonist expression in a murine granulosa cell tumor model. *Cancer Res* 2006; **66**: 1964–1973.
45 Albrecht KH, Eicher EM. Evidence that Sry is expressed in pre-Sertoli cells and Sertoli and granulosa cells have a common precursor. *Dev Biol* 2001; **240**: 92–107.
46 Rocha AS, Vidal V, Mertz M, Kendall TJ, Charlet A, Okamoto H *et al.* The Angiocrine Factor Rspondin3 Is a Key Determinant of Liver Zonation. *Cell Rep* 2015; **13**: 1757–1764.
47 Bingham NC, Verma-Kurvari S, Parada LF, Parker KL. Development of a steroidogenic factor 1/Cre transgenic mouse line. *Genesis* 2006; **44**: 419–424.
48 Svingen T, François M, Wilhelm D, Koopman P. Three-dimensional imaging of Prox1-EGFP transgenic mouse gonads reveals divergent modes of lymphangiogenesis in the testis and ovary. *PLoS ONE* 2012; **7**: e52620.

Supplementary Information accompanies this paper on the Oncogene website (http://www.nature.com/onc)